ELSEVIER

Surface and Coatings Technology 133–134 (2000) 307–313

SURFACE & COATINGS TECHNOLOGY

www.elsevier.nl/locate/surfcoat

Characterisation of $Ti_{1-x}Si_xN_y$ nanocomposite films

F. Vaz[a,*], L. Rebouta[a], P. Goudeau[b], J. Pacaud[b], H. Garem[b], J.P. Rivière[b], A. Cavaleiro[c], E. Alves[d]

[a] *Departamento de Física, Universidade do Minho, Campus de Azurém, 4810 Guimarães, Portugal*
[b] *Laboratoire de Métallurgie Physique, Université de Poitiers, 86960 Futuroscope, France*
[c] *ICMES-Faculdade Ciências e Tecnologia da Universidade de Coimbra, 3030 Coimbra, Portugal*
[d] *ITN, Deptartamento de Física, E.N.10, 2685 Sacavém, Portugal*

Abstract

$Ti_{1-x}Si_xN_y$ films were synthesised by RF reactive sputtering from Ti and Si elemental targets, in an Ar/N_2 gas mixture. XRD results revealed the development of a two-phase system, composed of a nanocrystalline f.c.c. TiN (phase 1: B1 NaCl type) and a second one (phase 2), where Si atoms replaced some of the Ti ones, inducing a structure that we may call a solid solution. An amorphous phase, supposed to be of silicon nitride, within grain boundaries seems to be also present, especially for high Si contents. TEM experiments confirmed the f.c.c.-type structure for phase 2, which is the only phase that develops without ion bombardment. The higher lattice parameter of phase 1 (~ 0.429 nm compared to 0.424 nm for bulk TiN) may be explained by the residual stress effect on peak position. The Ti replacement by Si would explain the low value of the lattice parameter for phase 2 (~ 0.418 nm). All samples showed good results for hardness (Hv ≥ 30 GPa), and $Ti_{0.85}Si_{0.15}N_{1.03}$ at a deposition temperature of 300°C showed a value of approximately 47 Gpa, which is approximately double that of pure TiN. For higher deposition temperatures, an increase in hardness is observed, as demonstrated by this same sample, which at 400°C reveals a value of approximately 54 GPa. Similar behaviour was observed in adhesion, where this same sample revealed a critical load for adhesive failure of approximately 90 N. In terms of oxidation resistance, a significant increase has also been observed in comparison with TiN. At 600°C, the oxidation resistance of $Ti_{0.70}Si_{0.30}N_{1.10}$ is already 100 times higher than that of TiN. For higher temperatures this behaviour tends to be even better when compared with other nitrides. © 2000 Elsevier Science S.A. All rights reserved.

Keywords: Ti–Si–N; Titanium and silicon nitride; Hardness; Adhesion; Oxidation resistance; Texture

1. Introduction

The search for new superhard materials is increasing considerably. One of the fundamental concepts is based on Cohen's theoretical approach, regarding the dependence of the bulk modulus of a material on the strength of inter-atomic bonds [1]. Within this approach, it was predicted that C_3N_4 hardness should be close to that of diamond; however, the results revealed that it does not exceed 30 GPa [2]. On the other hand, non-stoichiometric structures composed of these two elements (CN_x) reached values between 50 and 60 GPa, illustrating that beyond bonds, the microstructure, which varied from amorphous in the former to turbostatic-type in the latter, is certainly determinant in this hardening process [3].

Based on this assumption, and in a set of simple and well-established rules [4,5], S. Veprek developed a new concept for producing superhard materials, of which the basic idea is to avoid the usual mechanisms leading to the fracture of crystalline (multiplication, movement and pile-up of dislocations) and amorphous (growth of microcracks) materials [3]. This idea involves the preparation of a two-phase system, composed of a nanocrystalline material embedded in an amorphous matrix; where (TM,Si)N (TM = transition metal, e.g. Ti, V, W, etc.) is one of the most well known. One particularly

* Corresponding author.

0257-8972/00/$ - see front matter © 2000 Elsevier Science B.V. All rights reserved.
PII: S0257-8972(00)00947-6

interesting case is that of Ti–Si–N, which has been mostly prepared by plasma assisted chemical vapour deposition (PACVD) techniques [6], although they were primarily prepared by physical vapour deposition (PVD) (reactive sputtering) from composite targets (Ti_xSi_y) [7]. These film structures resulted in a two-phase alloy of TiN grains embedded in an amorphous matrix of silicon nitride [6,7]. The outstanding values of hardness in these systems (higher than 50 GPa) has attracted the attention of several research teams.

Regarding the explanations for such outstanding behaviour, and especially the relationship to the developed microstructure [8], it is necessary to perform detailed structural analysis, namely to identify the type of phases that are developed. The investigation of its relation with the deposition technique, as well as the particular deposition conditions, are two of the most important issues to be clarified. The claimed two-phase nc-TiN/a-Si_3N_4 mixture [3] is far from being the systematic structure obtained from the deposition process, namely from reactive magnetron sputtering. Furthermore, it is clear from the published works [2,3,6,7,9] that the knowledge of the mechanisms that explain the observed behaviour, either physical or mechanical, is yet insufficient. This is the main purpose of this work, which consists of the preparation of $Ti_{1-x}Si_xN_y$ coating and the study of its structural and mechanical property relationships.

2. Experimental

Single crystal silicon ({100}) wafers and polished high-speed steel (AISI M2) substrates were used for the deposition of $Ti_{1-x}Si_xN_y$ samples. The films, with thickness ranging from 1.3 to 3.3 μm, were prepared in an ALCATEL SCM650 apparatus by RF reactive magnetron sputtering in an Ar/N_2 gas mixture, and with DC bias voltages ranging from −75 to +25 V. High purity Ti and Si targets, a constant substrate holder rotation of 4 rev./min, and temperatures ranging from 200 to 500°C were used. In order to enhance the adhesion, a Ti adhesion layer of approximately 0.35 μm was deposited on the substrates prior to depositions. Rutherford backscattering spectrometry (RBS) and 'ball cratering' (BC) experiments were used to determine the atomic composition and thickness of the samples, respectively. X-Ray diffraction (XRD) and transmission electron microscopy (TEM) were used for structure characterisation. XRD diagrams were recorded in a SIEMENS D5000 diffractometer (CuK_α) using the conventional Bragg–Brentano Θ–2Θ configuration. TEM observation was performed in both conventional (JEOL 200CX) and high-resolution modes (JEOL JEM3010), with accelerating voltages of 200 and 300 kV, respectively. The samples were prepared by the microcleavage technique.

The hardness experiments were carried out in a Fischerscope H100 ultramicrohardness tester, equipped with a Vickers diamond indenter. The applied load was increased in 60 steps (the same for unloading) until the nominal load reached 30 mN (maximum load in all tests). The system had a load resolution better than 1 μN and the range of the nominal test load is between 4 mN and 1 N. The indentation depths were obtained with an accuracy of 2 nm. Fifteen tests were performed in each sample, with an additional ten for samples with high dispersion in the results. A careful procedure for test calibration was used, as outlined in [10,11].

In adhesion characterisation, scratch tests were performed in a computer-controlled Sebastian Five-A (Quad group) scratch tester. The tests were conducted with fixed standard conditions, using a 200-μm diamond tip, a constant scratching speed of 10 mm/min and a loading rate of 100 N/min. An average number of five tests were performed in each sample.

The oxidation resistance experiments were performed in air in a furnace, for temperatures ranging from 500 to 900°C and annealing times varying from 15 min to 9 h. The depth concentration profiles after annealing were measured by RBS. Experimental spectra were fitted using the RUMP program [12].

3. Results

Detailed information in terms of sample composition, thickness and grain size (vertical coherence width) evaluation can be found in [10].

3.1. Structural characterisation

The results revealed a mixture of two phases (Fig. 1), where the so-called phase 2 is the only one formed under no bombardment of the growing film (bias voltage ≥ 0). Regarding phase 1, the results reveal the development of a f.c.c.-type structure (B1 NaCl), with a lattice parameter of approximately 0.429 nm [10], with small variations according to variations in stress states [13]. By XRD, the exact nature of phase 2 was difficult to evaluate, since in most cases only one family peak is clearly visible [10]. However, TEM observation of a sample ($Ti_{0.80}Si_{0.20}N_{1.07}$) prepared with a bias voltage of +25 V (revealing only phase 2) has confirmed that phase 2 is also of a f.c.c.-type structure, as demonstrated on Fig. 2. The simulation of the diffraction rings was performed taking into account a f.c.c.-type structure, resulting in a lattice parameter close to that obtained in XRD. In Fig. 2a, a grain larger than 15 nm is clearly visible, although the large grain sizes involved

in these samples makes an accurate evaluation difficult, because of the possible superposition of different grains. The separation of these two phases, although quite simple by XRD, becomes extremely difficult to fulfil in electron microscopy, due to the small differences in the inter-atomic spacing. This fact implies that in diffraction mode, the possible existence of two distinct rings for each reflection could appear as only one (although thicker). However, the existence of two distinct types of grain observed under high resolution, although not certain, could be an indication of this mixture. Fig. 3 shows two micrographs of a $Ti_{0.63}Si_{0.37}N_{1.12}$ coating, where these two types of grain are clearly visible. This kind of grain mixture was never observed in samples with only phase 1 present, namely pure TiN. In the rings of the first image, the growth direction is also pointed out (significant brightness increase in some parts of the ring), revealing the ⟨200⟩ preferential growth, which could be proved in cross-section observation that it was parallel to the substrate surface. This result confirms that obtained by XRD [10]. Although the bigger grain, attributed to phase 2, is smaller than those of this same phase in the unbiased samples, the ion bombardment ($V_{bias} = -50$ V) and/or superposition between that and other grains might explain this result.

In order to have further information regarding this phase mixture, and specifically that referred to as phase 2, extended EXAFS experiments are currently being performed on these samples, and the preliminary results seem to confirm this Si introduction in the TiN matrix [14].

3.2. Mechanical characterisation

3.2.1. Hardness

Fig. 4a shows the dependence of hardness on the Si content. Fig. 4b shows the variation in hardness as a function of the applied bias voltage. As is clear from Fig. 4a, the addition of Si improves the hardness of TiN, with this hardening effect being more pronounced for Si contents of approximately 7 at.% (deposition temperature of 300°C). This behaviour is in accordance with the foregoing investigations in other groups [3,9], and is consistent with the formation of TiN nanocrystals embedded in an amorphous silicon nitride tissue. The beneficial effects of this structural arrangement reach a maximum for this region of compositions, which can be explained by taking into consideration the nanocomposite structure described by Veprek [3], based on the theoretical approach of R. Hertzberg [4] and A. Kelly [5]. For higher Si contents, the hardness becomes quite similar to that of Si_3N_4 [9], which is also consistent with the increase in the amorphous matrix referred to. These results are also consistent with previ-

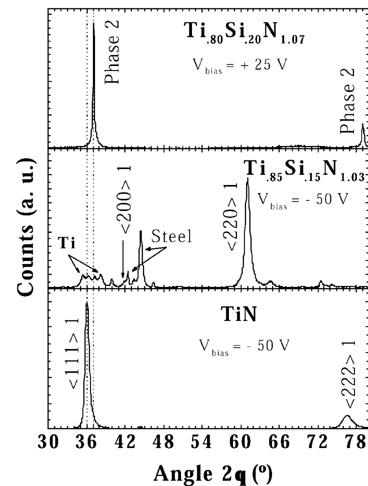

Fig. 1. Example of XRD diffraction patterns of $Ti_{1-x}Si_xN_y$ films illustrating the two crystalline phases that are developed.

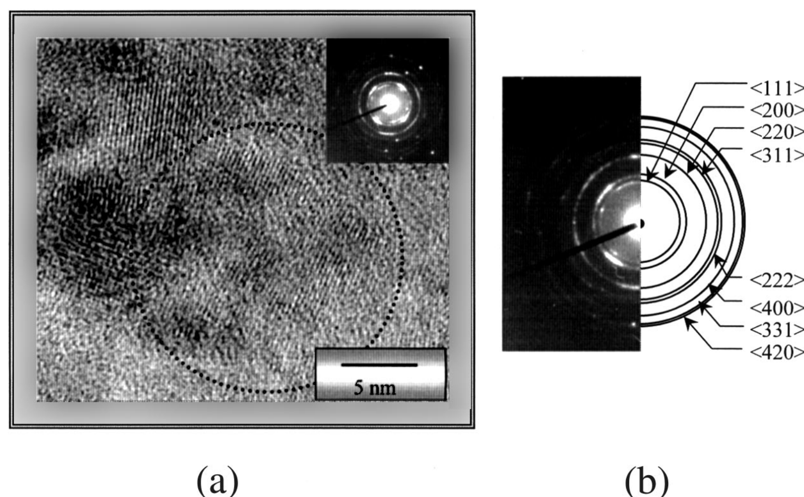

Fig. 2. (a) High-resolution transmission electron microscopy image (HRTEM) from $Ti_{.80}Si_{.20}N_{1.07}$ ($V_{bias} = +25$ V); and (b) corresponding diffraction rings.

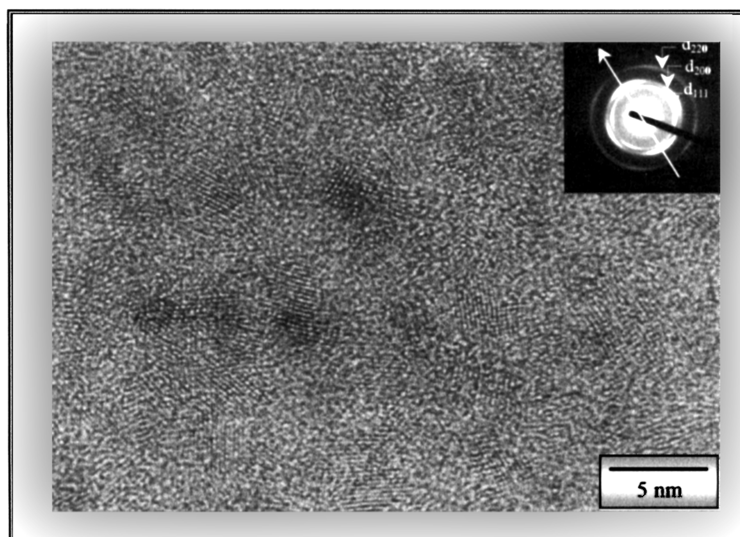

(a)

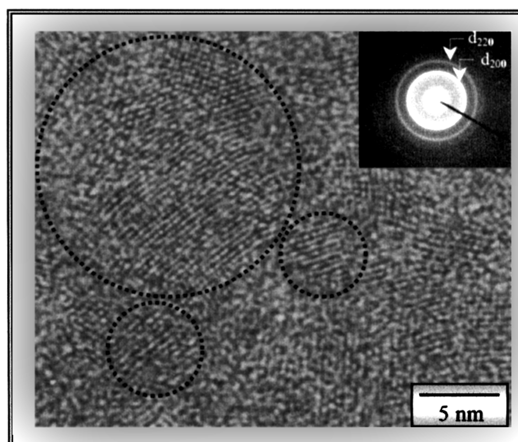

(b)

Fig. 3. HRTEM images from $Ti_{.63}Si_{.37}N_{1.12}$ fragments prepared by the microcleavage technique.

ous results obtained on nanocomposite materials, such as NiTi(N) deposited by ion beam assisted deposition [15,16], which is composed of TiN nanocrystals embedded in an amorphous matrix. It has been shown that the hardness and wear improvements depended on both the nanograin size and the composition of the amorphous matrix.

The low values of hardness for samples prepared with a positive bias voltage, where the diffraction patterns revealed only the formation of phase 2 and grain size values of approximately 23–30 nm [17], can be explained by the particular structure that is developed in these samples. The development of this structure can be explained by the low deposition temperature (300°C), together with the absence of ion bombardment, which does not provide the necessary mobility of the species at the growing film in order to ensure phase segregation and the consequent formation of polycrystalline grains and the amorphous matrix. These are probably the main events that could explain the formation of that phase, which might be the so-called solid solution. Furthermore, the presence of this phase 2 is certainly a factor to take into account, as it is reflected in the results of hardness as a function of temperature, Fig. 5a. Although the Si contents are relatively high, a significant increase in hardness is clearly visible. The presence of phase 2, clearly visible at 200°C, Fig. 5b, disappears progressively as the temperature is raised, probably due to an enhancement in species mobility at the growing film and/or changes in ion-to-atom flux ratios. This increase in mobility is then enough to ensure the nanocrystal/amorphous phase segregation, enhancing the hardening benefits attributed to this structural arrangement [3].

In spite of the high Si content in the sample prepared at 500°C (14.0 at.%), a hardness value of approximately 49 GPa is obtained. The more effective phase segregation certainly plays the most important role, since in the case of $Ti_{0.85}Si_{0.15}N_{1.05}$, which showed the highest hardness value at 300°C (47 GPa), showed a value of approximately 54 Gpa at 400°C, but without any traces of phase 2, which was present at 300°C (Fig. 1).

3.2.2. Adhesion

Three types of critical loads were identified: L_{C1} being the first cohesive failure, L_{C2} the first adhesive failure and L_{C3} the load at which more than 50% of the coating was removed from the substrate. The evaluation of these adhesion loads was achieved by the conjugation of optical observation with the variations in the acoustic emission signal and the inflection in the friction force curve [18]. Fig. 6 shows the dependence of these adhesion loads on the Si content and deposition temperature.

The similarity between the behaviours shown by these graphs and those of hardness, implies that the mechanisms of property improvement are basically the same. The result at 2.5 at.% Si (Fig. 6a) is somewhat unusual, which could be the result of two main factors: the large difference in failure mechanisms revealed by the samples in this composition region [18], and significant stress reduction revealed by this sample [13]. Similar

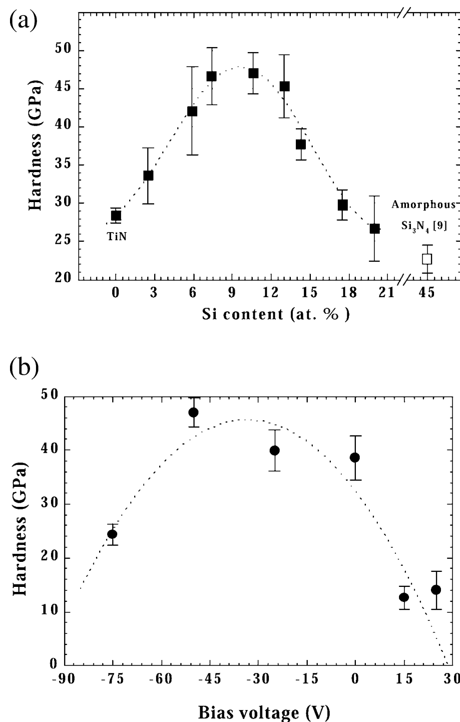

Fig. 4. Ultramicrohardness values of $Ti_{1-x}Si_xN_y$ samples as a function of: (a) Si content (−50 V bias voltage); and (b) bias voltage (300°C substrate temperature).

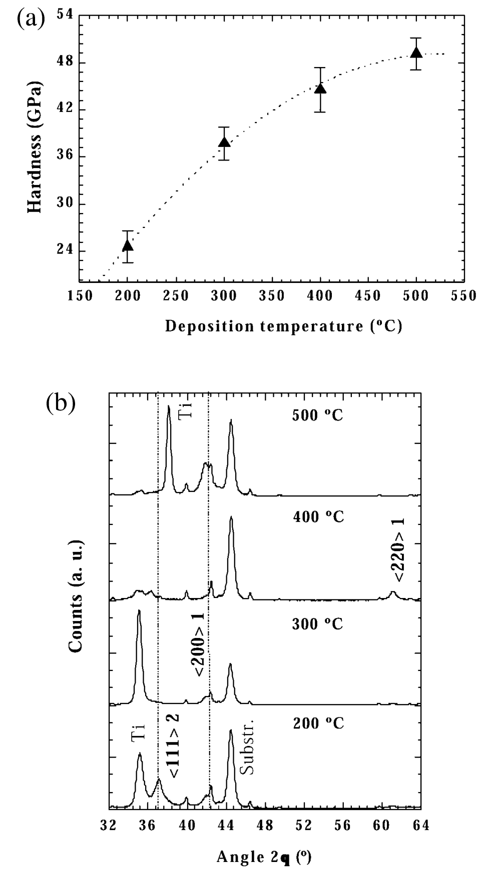

Fig. 5. (a) Ultramicrohardness values of $Ti_{1-x}Si_xN_y$ samples as a function of temperature; and (b) corresponding diffraction patterns. The Si contents in these samples are 15.2, 14.3, 13.4 and 14.0 at.% at 200, 300, 400 and 500°C, respectively.

behaviour was observed in two other samples prepared with the same deposition parameters and revealing the same composition.

3.3. Oxidation resistance

Fig. 7a shows the variation in oxidation resistance at a temperature of 800°C, and in comparison to other nitrides that reveal good oxidation resistance performance [19,20].

Despite the fact that the oxidation resistance of this $Ti_{1-x}Si_xN_y$ system cannot be considered outstanding, the observed results show a clear increase in oxidation resistance with increasing Si content. For small Si additions, and although an improvement is observed when compared to TiN, almost all the coating is oxidised for oxidation times greater than 2 h. For higher Si additions, this behaviour is considerably improved. For 1 h at 600°C, the oxidation resistance of $Ti_{0.70}Si_{0.30}N_{1.10}$ is already approximately 100 times higher than that of TiN [21,22], but approximately 10 times lower than that of $Ti_{0.35}Al_{0.65}N$, for which the best oxidation resistance behaviour was observed in the (Ti,Al)N system [19,20].

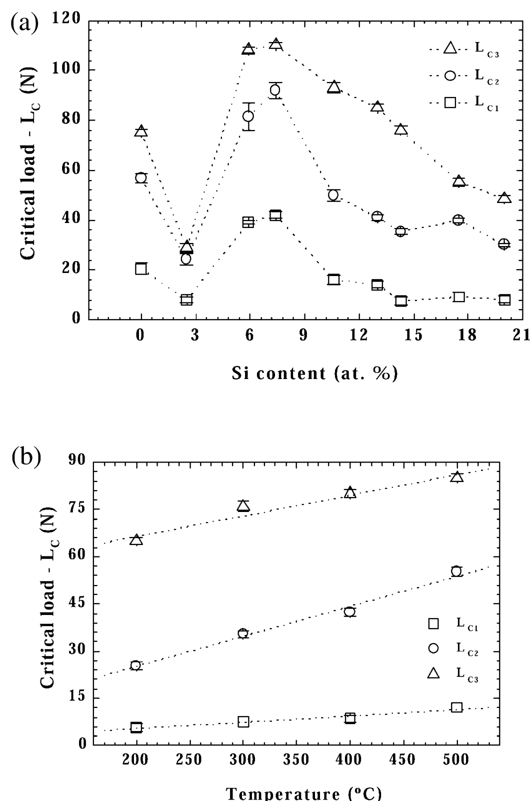

Fig. 6. Critical adhesion loads for the $Ti_{1-x}Si_xN_y$ samples as a function of: (a) Si content; and (b) deposition temperature.

With increasing temperatures (1-h oxidation), Fig. 7b), this difference tends to decrease slightly. For 1 h at 850°C, for instance, the oxidation resistance of $Ti_{0.70}Si_{0.30}N_{1.10}$ is only approximately three-fold lower than that of $Ti_{0.35}Al_{0.65}N$. The comparison with TiN is inappropriate for these temperatures, as total oxidation is observed in this material. This improvement decreases in importance with increasing oxidation time, as illustrated by the result at 9 h (Fig. 7a), where the difference between samples referred to is already approximately a factor of four. For higher oxidation times, this difference increases even more [19,20].

On the contrary to what has been observed for hardness and adhesion, these results reveal that a progressive improvement is observed with an increase in the Si content. The large amount of grain boundaries (small grain size) and the presence of the amorphous matrix at grain boundaries with the corresponding formation of silicon oxide (SiO_2) reduces the oxygen diffusion, and are thus the main parameters which account for the observed behaviour.

4. Conclusions

Thin films within the (Ti,Si)N ternary system were prepared by RF reactive magnetron sputtering. XRD results showed that these coatings are principally composed of a two-phase mixture, with a structure close to that of TiN. An amorphous silicon nitride material is also developed between the grain boundaries. A lattice parameter of approximately 0.429 nm was deduced for phase 1. Regarding phase 2, the results obtained by both XRD and TEM analysis indicate that this is also a cubic lattice, where some of the Si atoms are occupying Ti positions. A lattice parameter of approximately 0.418 nm for this phase would result from this assumption. Fourier analysis on the X-ray diffraction patterns revealed a nanocrystalline nature of the developed grains (4–7 nm), confirmed by HRTEM micrographs. This mixture of phases is closely related to the applied substrate bias, since phase 2 was the only one observed for conditions where no bombardment of the growing film was present. The low deposition temperature and deposition rate, and the absence of this ion bombardment induce low species mobility at the growing film that cannot efficiently segregate the nanocrystal-

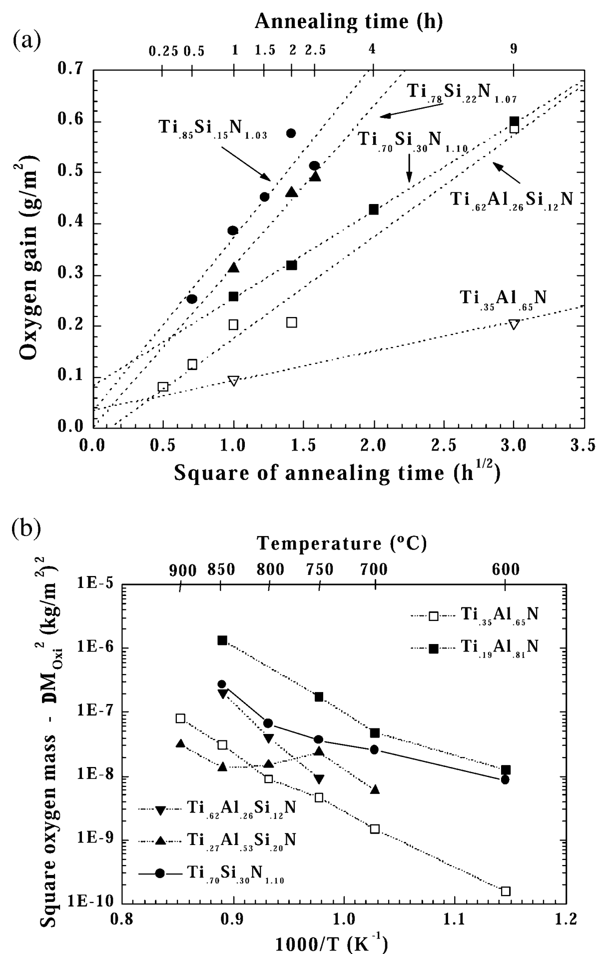

Fig. 7. Mass square of incorporated oxygen atoms as a function of: (a) time for an oxidation temperature of 800°C; and (b) annealing temperature for an oxidation time of 1 h. The results for $Ti_{1-x}Si_xN_y$ are compared with others from other nitride systems prepared in our laboratory [18,19].

line/amorphous phase-type structure. An increase in temperature is known to induce a more efficient phase segregation, resulting in an enhancement of mechanical properties, ruled by the two-phase structure described by Veprek [3]. These benefits were particularly apparent in hardness values, where an increase in temperature (300 to 400°C) corresponded to an increase from 47 to 54 GPa for $Ti_{0.85}Si_{0.15}N_{1.03}$ (which revealed the best hardness values at 300°C). Similar behaviour was observed for higher Si contents. In terms of adhesion, the behaviour is similar to that of hardness, revealing critical adhesion loads for adhesive failure as high as 90 N. Higher Si additions induce a behaviour close to that of amorphous silicon nitride, which might be a consequence of the significant increase in the amorphous phase of these structures. The oxidation resistance is also improved for large Si additions, which can be explained by the same arguments (i.e. an increase in the amorphous phase volume fraction).

Acknowledgements

The authors gratefully acknowledge the financial support of the French/Portuguese CNRS/ICCTI institutions, through programs no. 5522 (1998) and no. 7087 (1999).

References

[1] M.L. Cohen, Solid State Commun. 92 (1994) 45.
[2] S. Veprek, J. Weidemann, F. Glatz, J. Vac. Sci. Technol. A 13 (1995) 2914.
[3] S. Veprek, Surf. Coat. Technol. 97 (1997) 15 (And references therein).
[4] R. Hertzberg, Deformation and Fracture Mechanics of Engineering Materials, 3rd, Wiley, New York, 1989.
[5] A. Kelly, N.H. MacMillan, Strong Solids, 3rd, Clarendon, Oxford, 1986.
[6] S. Veprek, S. Reiprich, L. Shizhi, Appl. Phys. Lett. 66 (1995) 2640.
[7] X. Sun, J. Reid, E. Kolawa, M.-A. Nicolet, J. Appl. Phys. 81 (2) (1997) 656.
[8] F. Vaz, L. Rebouta, B. Almeida et al., Surf. Coat. Technol. 120/121 (1999) 166.
[9] M. Diserens, J. Patscheider, F. Lévy, Surf. Coat. Technol. 120/121 (1999) 158.
[10] F. Vaz, L. Rebouta, S. Ramos, M.F. da Silva, J.C. Soares, Surf. Coat. Technol. 108/109 (1998) 236.
[11] A.C. Trindade, A. Cavaleiro, J.V. Fernandes, J. Test. Eval. 22 (4) (1994) 365.
[12] L.R. Doolittle, Nucl. Instrum. Methods B9 (1985) 344.
[13] F. Vaz, L. Rebouta, R. Silva, M.F. da Silva, J.C. Soares, Vacuum 52 (1999) 209.
[14] F. Vaz, Ph.D. Thesis, Minho University, Portugal, 2000.
[15] K. Bouslykhane, P. Moine, J.P. Villain, J. Grilhé, Surf. Coat. Technol. 49 (1991) 457.
[16] T. Girardeau, K. Bouslykhane, J. Minault, J.P. Villain, P. Chartier, Thin Solid Films 283 (1996) 67.
[17] J. Mignot, S. Rondot, Acta Metall. 23 (1975) 1321.
[18] F. Vaz, L. Rebouta, M. Andritschky, M.F. da Silva, J.C. Soares, J. Mater. Proc. Technol. 92/93 (1999) 169.
[19] F. Vaz, L. Rebouta, M.F. da Silva, J.C. Soares, in: Y. Pauleau, P. Barna (Eds.), Protective Coatings and Thin Films: Synthesis, Characterization and Applications, Kluwer Academic Publishers, Dordrecht, 1996, p. 501.
[20] F. Vaz, L. Rebouta, M. Andritschky, M.F. da Silva, J.C. Soares, J. Eur. Ceram. Soc. 17 (1997) 1971.
[21] D. McIntyre, J. Noser, H. Melchior, J. Appl. Phys. 52 (1) (1981) 52.
[22] M. Wittmer, J. Noser, H. Melchior, J. Appl. Phys. 52 (11) (1981) 6659.